Study of the $a_2(1320)$ Meson in Two-Photon Collisions

The L3 Collaboration

Abstract

The two-photon production of $a_2(1320)$ meson has been studied by detecting the decay of $a_2 \rightarrow \pi^+\pi^-\pi^0$. The data corresponding to an integrated luminosity of 100.1 pb^{-1} were taken during 1992 to 1994 with the L3 detector at LEP. The fraction of a_2 helicity state $|\lambda|$=2 is determined to be 92. $\pm$ 7.%. The $\gamma\gamma$ width of the a_2 is found to be $\Gamma_{\gamma\gamma}(a_2) = 1.04 \pm 0.06 \pm 0.13$ KeV.

Submitted to the 1995 International Europhysics Conference on High Energy Physics, Brussels, Belgium, 27th July - 2nd August 1995.

1 Introduction

The formation of resonance in two-photon interaction at e^+e^- storage ring experiments provide informations to study the SU(3) multiplets of light mesons. The photons radiated by $e^\pm$ are quasi-real with very small emitting angle to the $e^\pm$ beam direction. The resonance produced via the exchange of two photons is required to be neutral with positive charge conjugation ($C = +1$) and the helicity restricted to $\lambda = 0, \pm 2$.

The $\gamma\gamma \to a_2$ production has been investigated by many experiment [1-7], and the quantum number is well established to be $J^{PC} = 2^{++}$ with predominantly helicity $|\lambda| = 2$. The $a_2 \to \rho\pi$ decay channel dominates with 70 % branching ratio. In this report we present the analysis on 3π final state of a_2 from the reaction chain

$$\begin{array}{lllllll} e^+e^- & \to & e^+e^- & a_2 & & & \\ & & & \hookrightarrow & \rho^\pm\pi^\mp & \to & \pi^+\pi^- \quad \pi^0 \\ & & & & & & \qquad\quad \hookrightarrow \gamma\gamma \end{array}$$

The data taken by the L3 experiment during 1992 to 1994 correspond to a total integrated luminosity of 100.1 pb^{-1}. We have studied the helicity state and radiative width of a_2 meson.

In section 2, we outline the detector components used in this analysis; the event selection is portraited in section 3 to obtain the mass spectrum of $\pi^+\pi^-\pi^0$ final state. The Monte Carlo simulation described in section 4 provides trigger efficiency and detector acceptance. The formation of resonance in the two-photon collision is described by the luminosity function of photon flux convoluted by the Breit-Wigner formula for the resonance production.

In the a_2 center of mass frame, the distributions of the $\rho^\pm$ and π^0 polar angles have helicity dependence. Described in section 5 is the least square minimization to the Monte Carlo distribution of helicity $|\lambda| = 0, 2$. The radiative width is determined with the event normalization to Monte Carlo prediction of helicity 2 state.

2 The L3 subdetectors for a_2 decay

The L3 detector [8] at LEP is suitable for two-photon resonance study. The charged pions are detected by the central TEC tracker, which is a cylindrical high resolution drift chamber of a polar angle acceptance $13^\circ \le \theta \le 167^\circ$ in a magnetic field of 0.5 T. The TEC chamber is divided into 96 sectors in the azimuthal angle ϕ. The sensitive region in radial direction is between 10 to 45 cm with 62 layers of wires to provide spatial resolution of $\simeq 50$ μm and p_T resolution $\sigma/p_T^2 = 0.02$ (GeV)$^{-1}$. The z-chamber surrounding TEC provides the track z coordinates. The SMD detector, that participated to the 1994 data taking, has two layers of silicon wafers around the beam pipe to provide high precision inner tracking points.

The photons from π^0 decay are detected by the electromagnetic calorimeter of about 11000 BGO crystals placed around the TEC to cover the barrel region of $42^\circ \leq \theta \leq 138^\circ$ and the two endcaps of $11.6^\circ \leq \theta \leq 38^\circ$. The energy resolution of the BGO calorimeter is $\simeq 5\%$ at 100 MeV and $\simeq 2.3$ % at 1 GeV.

The $\gamma\gamma \rightarrow a_2$ events are mainly taken by triggering on tracks with an angular coverage of $25^\circ \leq \theta \leq 155^\circ$ requiring at least one pair of tracks in TEC back to back within $\pm 41^\circ$.

3 Event selection

The final state particles are the scattered $e^\pm$ going mostly down the beam pipe. The low energy charged pions are detected by the TEC chamber and the neutral pion decay into two photons detected by BGO crystals. The loose selected two-photon samples are low multiplicity events with large missing energy in central detector.

The TEC chamber measures charged tracks with p_T threshold at 60 MeV. We require good tracks to have at least 20 TEC hits out of the total 62 layers of wires. The distribution of TEC hits of the two-photon sample is shown in Fig. 1. The BGO crystal cell size is 2×2 cm^2 that span over 2° in both θ and ϕ. The magnetic field is along z direction, the charged pions arriving at the BGO has deflection angle of $\Delta\phi = 0.3 \cdot 0.5\mathrm{T} \cdot r/p_T$. Applying $r = 0.28$ m, the matching in ϕ between TEC and BGO is shown in Fig. 2. The θ of matched BGO bumps are applied to the tracks to improve track momentum measurement. As the two charged pions come from 3-body decay, events are rejected if the opening angle of the two tracks is larger than 170° and the difference in ϕ angle is within $180 \pm 5^\circ$.

A photon detected by the BGO calorimeter is a neutral bump requiring the angular difference of $\sqrt{\Delta\theta^2 + \Delta\phi^2} > 5.5^\circ$ off TEC tracks, the event distribution is shown Fig. 3. The crystals near the edges of BGO detector have excessive events (Fig. 4); the fiducial cuts are $\theta < 14^\circ$ and $35^\circ < \theta < 45^\circ$ from the beam axis. The photon energy is required to be greater than 100 MeV.

To eliminate beam-gas contamination, the primary vertex of the two tracks are required to have the average and difference in DCA and z to be smaller than 2.5 and 50 mm respectively; Fig. 5 shows the vertex DCA and z after cuts.

The sample of $\pi^+\pi^-\pi^0$ final state are events of two tracks with opposite charge and two photons. In Fig. 6 the dE/dx distribution for negative-charged tracks is shown. The invariant mass spectrum of the two photons is shown in Fig. 7. The π^0 reconstructed from the two photons is required to have mass of $80 < m(\gamma\gamma) < 160$ MeV.

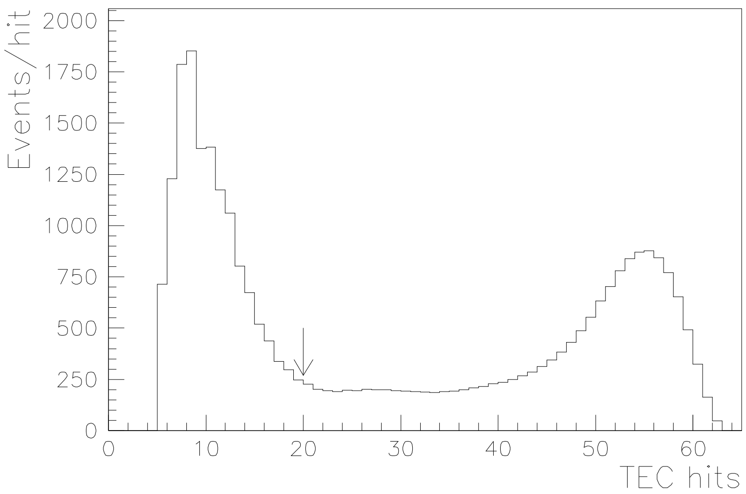

Figure 1: The TEC hits of two-photon loose selected sample.

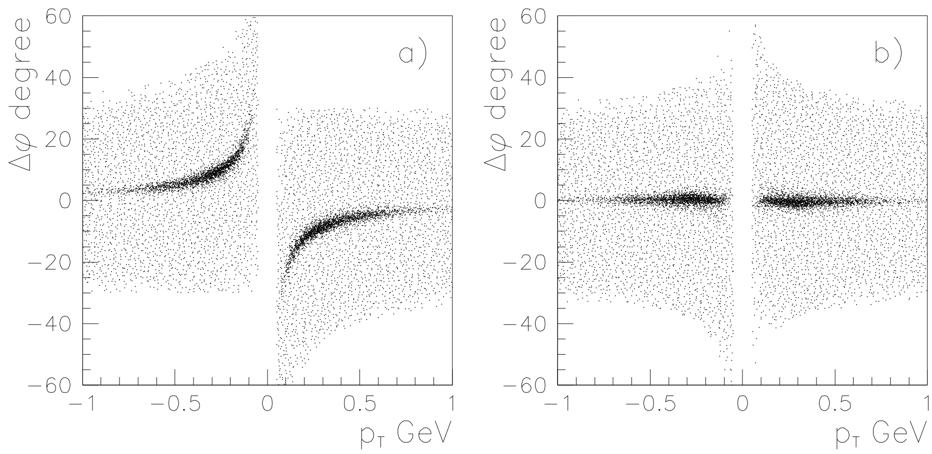

Figure 2: The difference in ϕ of tracks measured by TEC and BGO; a) no correction on field deflection, b) with field deflection corrected.

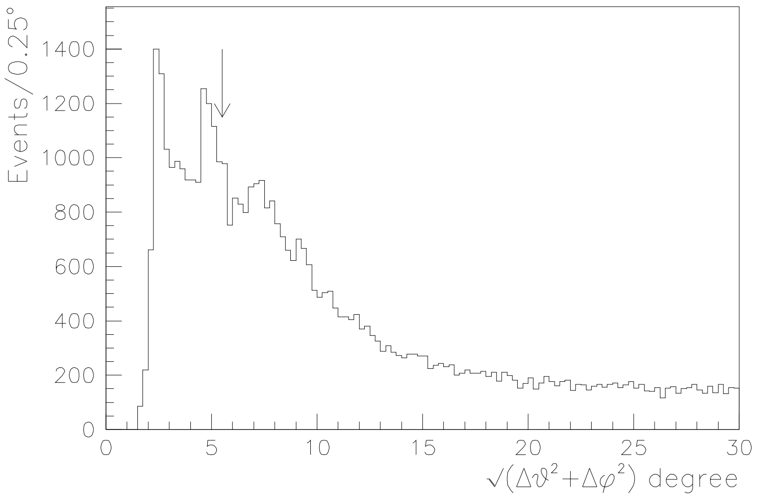

Figure 3: Distribution of $\sqrt{(d\theta^2 + d\phi^2)}$ of BGO photon to TEC track matched BGO bump.

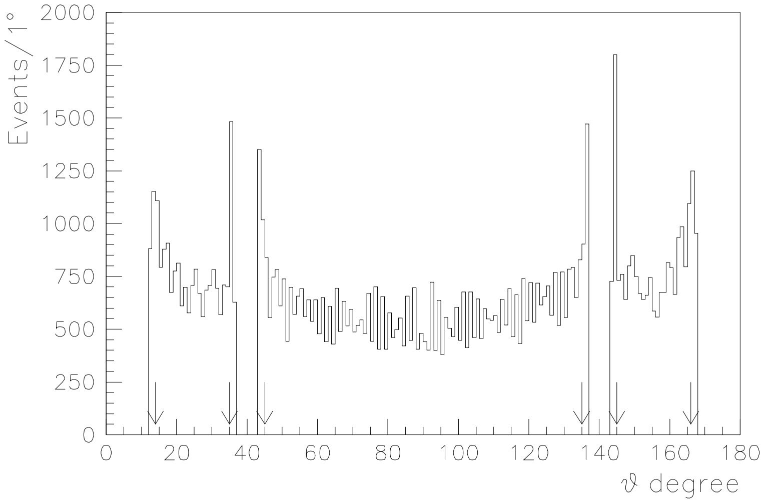

Figure 4: Distribution in θ of photons detected by BGO.

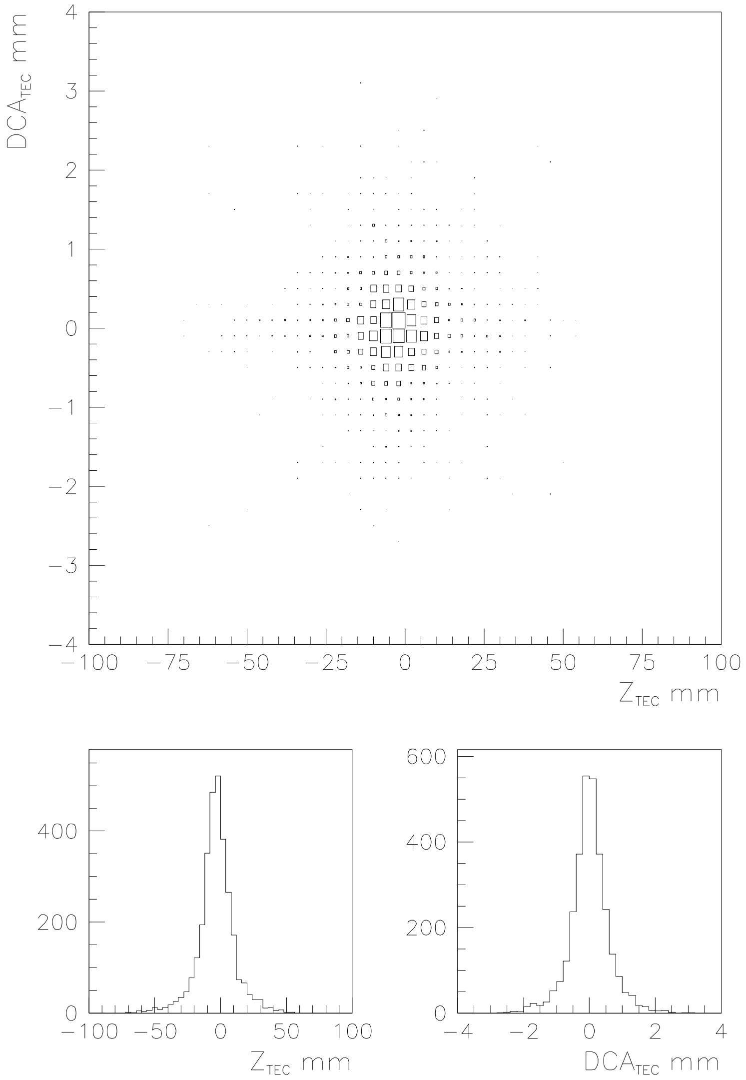

Figure 5: Distribution of track DCA versus z at primary vertex.

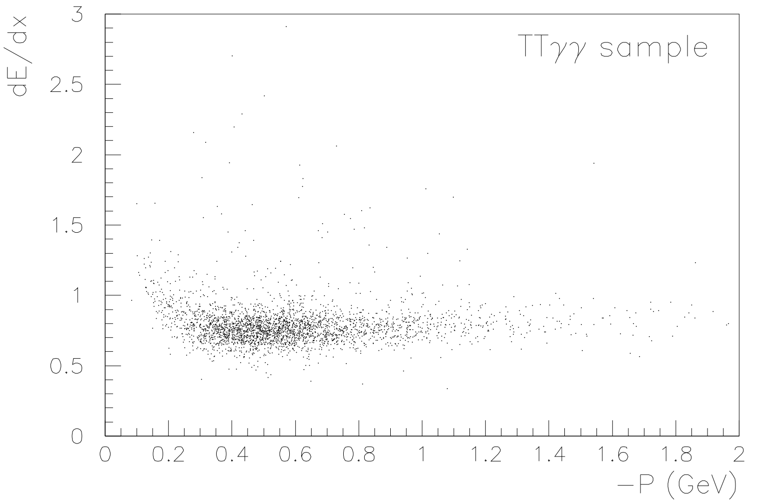

Figure 6: The dE/dx spectrum of negative-charged tracks.

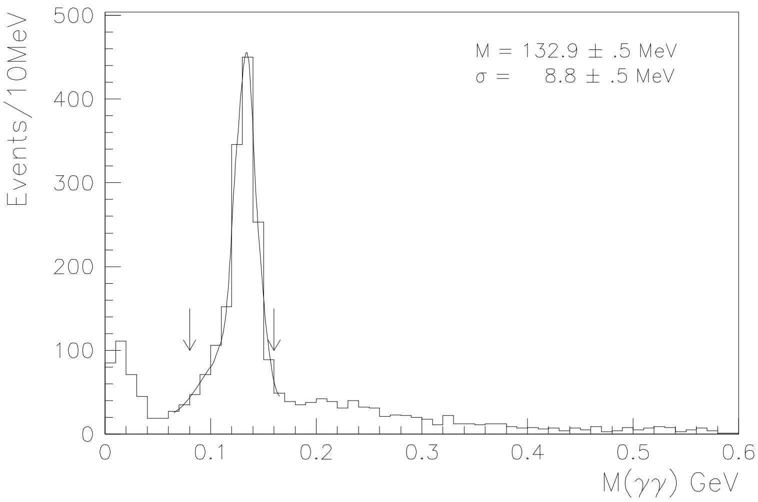

Figure 7: Invariant mass of the two final state photons; the fit of a Gaussian plus third order polynomial gives $m_{\pi 0} = 132.9 \pm 0.5$ MeV.

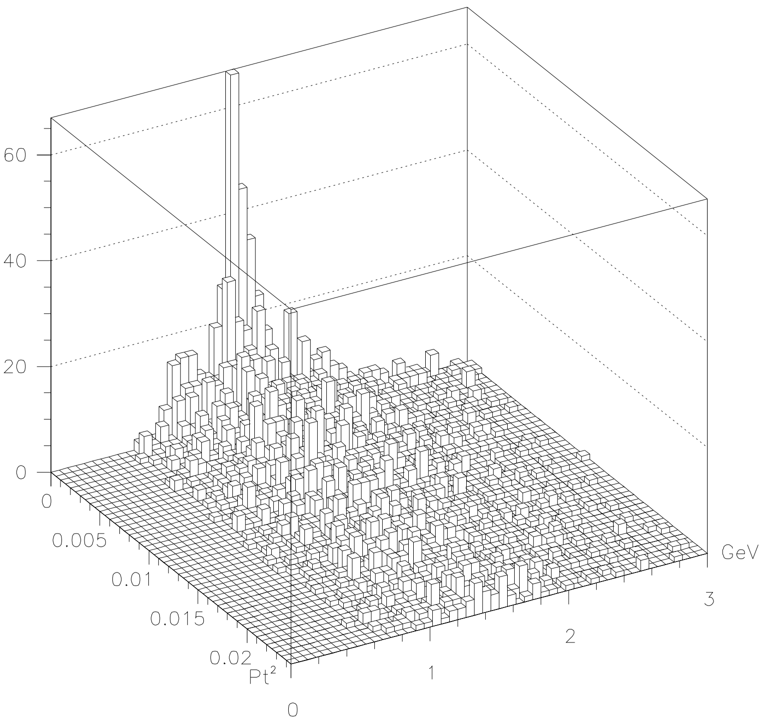

Figure 8: Distribution of $(\sum \vec{p}_T)^2$ versus invariant mass of $\pi^+\pi^-\pi^0$ sample.

The distribution of $(\sum \vec{p}_T)^2$ versus invariant mass $m(\pi^+\pi^-\pi^0)$ is plotted in Fig. 8. To suppress background, the $(\sum \vec{p}_T)^2$ is required to be smaller than 0.01 GeV^2; the $\rho^\pm$ intermediate state is reconstructed by combining $\pi^\pm$ and π^0. The $\rho^\pm$ invariant mass distribution is shown in Fig. 9; we require both ρ^+ and ρ^- masses to be smaller than $m_\rho + 250$ MeV.

The invariant mass spectrum of $\pi^+\pi^-\pi^0$ is shown in Fig. 10, in which the a_2 resonance is fitted by a Gaussian plus a background of third order polynomial. The histogram contains 793 events, after background subtraction the number of a_2 event is 473 ± 28. The a_2 mass and total width from the fit are $m_A = 1.307 \pm 0.01$ GeV and $\Gamma = 100.7 \pm 1.0$ MeV respectively.

4 Monte Carlo generation for a_2 resonance

We have applied Monte Carlo simulation to evaluate the detector acceptance for the determination of radiative width and the helicity dependence of a_2 coupling to two-photon. We have applied the PC [9] and TWOGEN [10] programs to calculate the luminosity function ($\mathcal{L}_{\gamma\gamma}$) of transverse photon flux

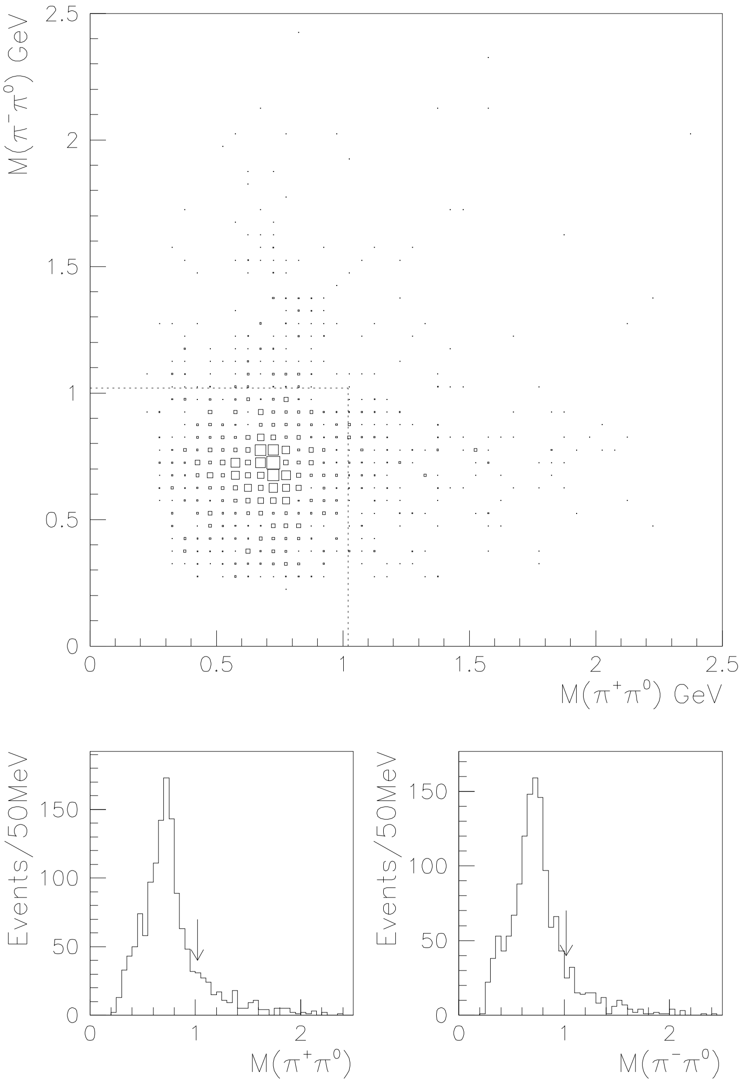

Figure 9: The $\rho^{\pm}$ invariant mass distribution.

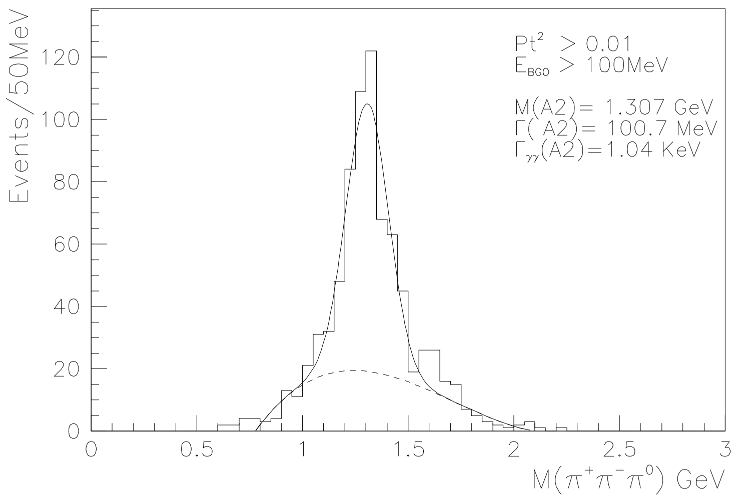

Figure 10: The invariant mass of $\pi^+\pi^-\pi^0$ and the fit to a_2 mass and width.

[11] from $e^+e^- \to e^+e^-\gamma\gamma$. The a_2 production is described by the product of the luminosity function and the differential cross section of $\gamma\gamma \to a_2 \to \rho\pi$. The intermediate state of $\rho^+\pi^-$ and $\rho^-\pi^+$ has constructive interference [12]. For the final 3π state the a_2 differential cross section is

$$
\begin{aligned}
d\sigma &= 2\pi(2J+1)\frac{m_A}{s}\frac{\Gamma_{\gamma\gamma}}{(m_A^2-s)^2+m_A^2\Gamma_A^2} \\
&\times \sum_\lambda R_{\lambda\lambda}\left|\frac{T_\lambda(a_2 \to \rho^+\pi^- \to 3\pi)}{m_\rho^2 - s_\rho^+ - im_\rho\Gamma_\rho^+} + \frac{T_\lambda(a_2 \to \rho^-\pi^+ \to 3\pi)}{m_\rho^2 - s_\rho^- - im_\rho\Gamma_\rho^-}\right|^2 \\
&\times d(\mathrm{LIPS})_{3\pi} \qquad (1)
\end{aligned}
$$

where $d(\mathrm{LIPS})_{3\pi}$ is the 3π Lorentz invariant phase space element; s is the 3π invariant mass squared, and $J(\lambda)$ is the a_2 spin(helicity). $s_\rho^\pm$ is the $\pi^\pm\pi^0$ invariant mass squared. The a_2 mass (m_A) and total width (Γ_A^0) come from PDG [13]. The mass dependence of a_2 width is given by [14]

$$\Gamma(s) = \Gamma^0\left(\frac{p}{p^0}\right)^{2L+1}\frac{D_L(p^0r)}{D_L(pr)} \qquad (2)$$

where $p^0(p)$ is the ρ momentum in the 3π rest frame with invariant mass equals $m_A(\sqrt{s})$, r =1 fm is the interaction range [15]; and D_L is the barrier penetration factor [16], $L = 2$ is the orbital angular momentum for $a_2 \to \rho\pi$.

Parameters of the ρ meson also have mass (m_ρ) and width (Γ^0_ρ) coming from PDG, and the energy dependent width is given by eq. 2 with $L = 1$ and $r = 0.58$ fm [17].

The relative helicity density is given by $R_{\lambda\lambda}$. The interacting photons are quasi-real, thus they do not couple to $\lambda = \pm 1$. Theoretical arguments suggests that helicity $|\lambda| = 2$ dominates [18].

The transition amplitude for $a_2 \to \rho\pi \to 3\pi$ of helicity λ is given by

$$\begin{aligned} T_\lambda &= 32\pi^2 (m_A \Gamma_A m_\rho \Gamma_\rho \frac{\sqrt{s s_\rho}}{p_\rho p_\pi})^{1/2} \\ & \times \sum_m C^{L\lambda}_{L,\lambda-m,1,m} Y_L^{\lambda-m}(\theta_\rho, \phi_\rho) Y_1^m(\theta_\pi, \phi_\pi) \end{aligned} \tag{3}$$

where m is the third component of the ρ spin, the spherical harmonic products is multiplied by the Clebsch-Cordan coefficients $C^{J,\lambda}_{L,\lambda-m,1,m}$. The ρ meson momentum, polar and azimuthal angles ($p_\rho, \theta_\rho, \phi_\rho$) are measured in the a_2 rest frame; and the π^0 from ρ decay has the corresponding variables (p_π, θ_π, ϕ_π) measured in the ρ rest frame. Angles of both frame are determined with respect to the e^+e^- beam direction.

We have instrumented the programs PC and TWOGEN to generate $a_2 \to 3\pi$ production. Both generators calculates the 4-momentum of the $\gamma\gamma$ system according to the luminosity function. The kinematic variables of final state particles are compared and agree well.

Combining the $\pi^\pm$ and π^0 to form the $\rho^\pm$, the ρ Breit-Wigner width and the transition amplitude of eq. 1 are applied by hit and miss mechanism. The a_2 meson has known quantum number $J^{PC} = 2^{++}$; we generate events assuming the helicity state can be $|\lambda| = 0$ and 2. Shown in Fig. 11.a is the Breit-Wigner distribution of $a_2 \to 3\pi$ with phase space calculated by PC and helicity states $|\lambda| = 0, 2$ by TWOGEN. The momentum transfer carried by the quasi-real photons are $Q_i \simeq 2EE'(1 - \cos\theta_i)$. The ratio $x = Q^2/(Q^2 + W^2)$ is shown in Fig. 11.b; where $Q = Max(Q_1, Q_2)$ and W is the invariant mass of $\gamma\gamma$ system. The agreement in x gives confidence on $\mathcal{L}_{\gamma\gamma}$ calculation. The helicity dependence is seen in the π^0 and $\rho^\pm$ distribution in θ in the a_2 cms frame (Fig. 12), the helicity 0(2) state has π^0 favoring transverse(forward) direction; the $\rho^\pm$ distribution in θ has opposite feature.

The PC program has $\Gamma_{\gamma\gamma} = 1$ KeV, the total cross section of a_2 resonance at $\sqrt{s} = m_Z$ is calculated to be 1074 ± 36 pb. The Monte Carlo events were passed through a full detector simulation where particular care was given to the photon detection efficiency according to the time dependent data base, and the trigger efficiency calibrated by Bhabha events using energy trigger in comparison with the trigger simulation.

The TEC trigger of two charged pions requires acolinearity in azimuthal

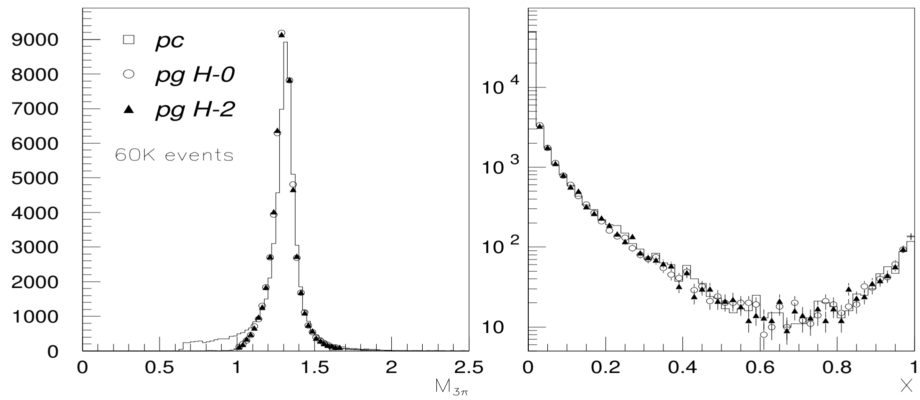

Figure 11: Comparison of the PC and TWOGEN generators. a) the mass spectrum; b) the x distribution.

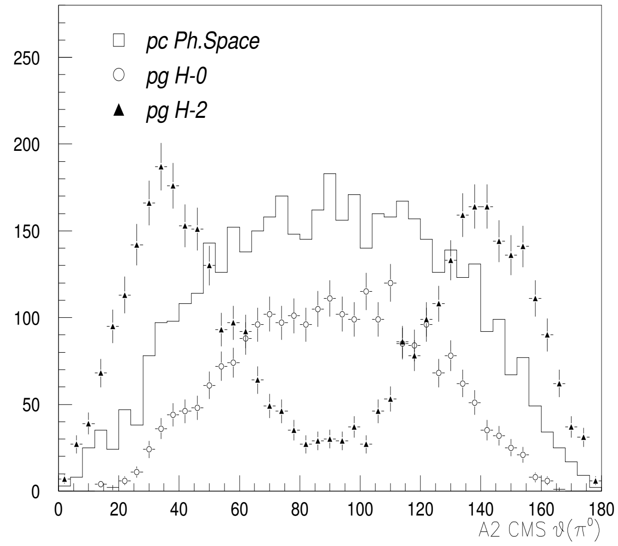

Figure 12: The helicity dependence of π^0 distribution.

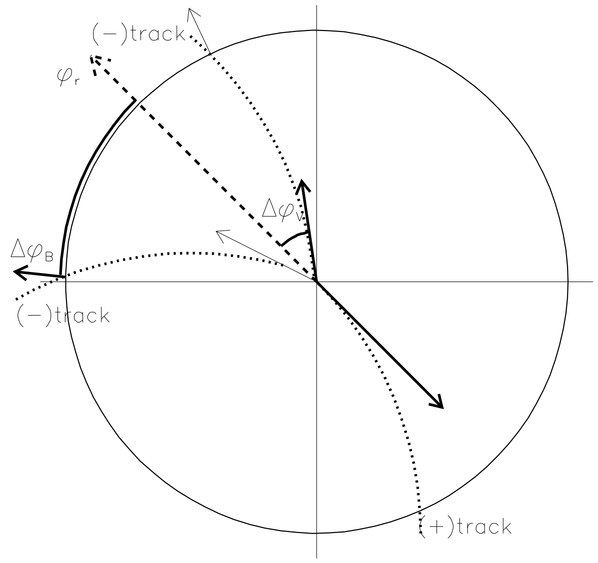

Figure 13: The field deflection of tracks in TEC.

angle which is complicated by the field deflection. In Fig. 13, the two opposite charged tracks are illustrated. Taking the reference ϕ_r as the opposite direction of positive charged at primary vertex, events fall in trigger coverage if
i) the negative track has $|\phi_r - \phi_V| < \Phi^-$ at vertex; or
ii) the negative track has $|\phi_r - \phi_B| < \Phi^+$ at BGO.

The TEC trigger is simulated using the parametrization on the Bhabha calibration by the following procedure
i) TEC trigger is assigned if $|\phi_r - \phi_V| < \Phi^-$, or $|\phi_r - \phi_B| < \Phi^+$;
ii) a flat random toss to meet the efficiency of Bhabha calibration in θ.

To have sufficient statistics, the loose selected 3π sample are used for comparison with the TEC trigger simulation. The $\Phi^\pm$ angle is determined to be Φ^+=Φ^-=45° as illustrated in Fig. 14, this also consists with the trigger simulation. The TEC calibration by Bhabha events has the efficiency distribution in θ (solid line) shown in Fig. 15 in comparison with data(circle). At $\theta = 40°$, the energy trigger is blank as it is the gap between BGO barrel and endcaps; and the two-photon event rate is lower due to the Level 2 to Level 3 trigger suppression and event selection efficiency. The bin content of Bhabha calibration at $\theta = 40°$ is adjusted after normalization to agree with the two-photon sample. The global TEC trigger rate of the simulation applying Bhabha calibration of 1992 and 1993 shows that the discrepancy between the years is smaller than 1%.

The acolinear angle of the two charged pions has helicity dependence.

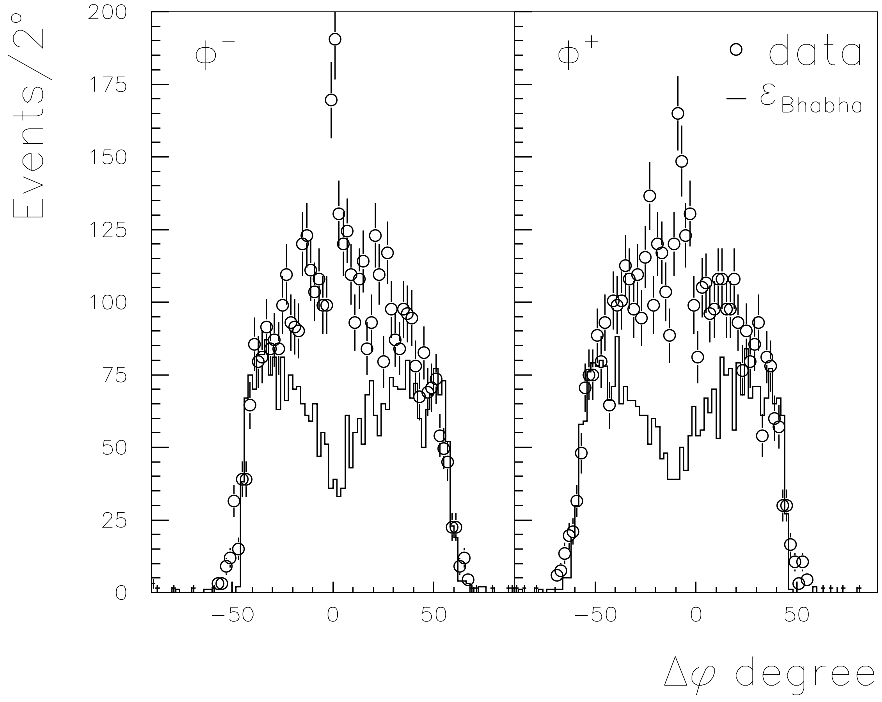

Figure 14: TEC trigger simulation in comparison with loose selected 3π events for the determination of $\Phi^{\pm}$, which are Φ^{+}=Φ^{-}=45°.

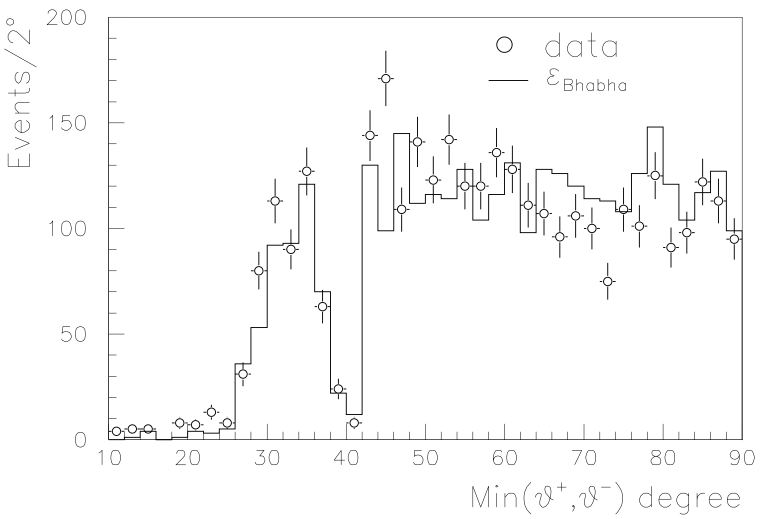

Figure 15: TEC trigger simulation in θ in comparison with loose selected 3π events; the track of lower θ is filled.

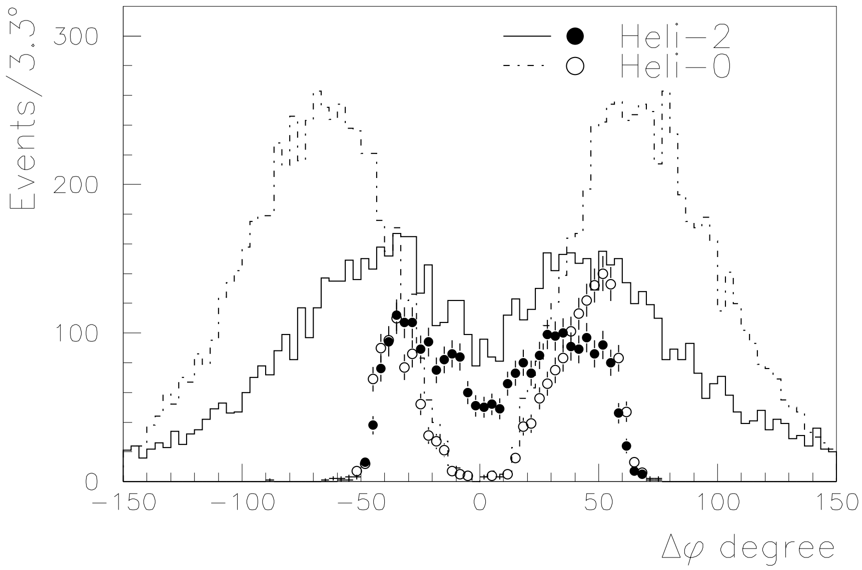

Figure 16: Simulation of TEC trigger before(lines) and after(circles) the back to back constraint on tracks.

Shown in Fig. 16 is the trigger simulation for a_2 helicity of 0(2) before and after applying the back to back constraint. For each helicity assignment ($|\lambda| = 0, 2$), the total of 362500 events were simulated. The Ideal detector acceptance were calculated using full detector simulation of 1993 detector setup with the values listed in Table 1.

		Heli-0	Heli-2
Without	TEC-trig	3.23%	2.33
With	TEC-trig	0.49%	0.65

Table 1: The Ideal detector acceptance.

The BGO efficiency has time dependence. We use a real detector simulation by applying the data base to mask off dead crystals with the corresponding integrated luminosity. The efficiency obtained are ε_{BGO}= 93.4%, 93.3% and 93.3% for 92,93 and 94 respectively; the average of 93.3% is applied to the Monte Carlo.

The number of expected a_2 events is

$$N_{MC} = \int \mathcal{L}_{ee} \times \sigma(ee \to eea_2) \times BR(a_2 \to \rho\pi) \times \varepsilon_{BGO} \times Acceptance \quad (4)$$

Corresponding to $\Gamma_{\gamma\gamma}(a_2)$=1 KeV, the numbers calculated in comparison with data are listed in Table 2.

N_{MC}^{Heli-0}	N_{MC}^{Heli-2}	N_{data}
344±34	456±46	473±28

Table 2: Number of events corresponding to 100.1 pb^{-1}.

5 The a_2 helicity and radiative width

In the a_2 cms frame, the three polar angle distributions of π^0, ρ^+ and ρ^- depend on the a_2 helicity. In Fig. 17 the data are the final selected sample of 793 events; the Monte Carlo events of different helicity have been scaled to the theoretical expectation in Table 2. We apply the least square minimization on

$$\chi^2 = \sum_{bin} \left\{ D_i - \left[P_c + P_s \cdot \left((1 - P_2) N_{MC\,i}^{Heli-0} + P_2 N_{MC\,i}^{Heli-2} \right) \right] \right\}^2 / D_i \qquad (5)$$

where D_i is the data content of the ith-bin in $\cos\theta$, and $N_{MC\,i}^{Heli-0}$,$N_{MC\,i}^{Heli-2}$ are the corresponding MC expectation at $\Gamma_{\gamma\gamma}(a_2)$=1 KeV for an integrated luminosity of 100.1 pb^-1. Here we assume that the background has a constant level (P_c), and the ratio of helicity-2 over helicity-0 events is P_2. The factor P_s scales the sum of Monte Carlo events thus giving measurement of the radiative width. The χ^2 minimization searches for the best agreement to the data on all three distributions. The result of the fit gives a reduced χ^2 of 1.58 and the fitting parameters are

P_c	11.8 ± 1.4
P_s	1.03 ± 0.04
P_2	$0.92 \pm .07$

Fixing the a_2 helicity to $|\lambda|$=2, from Table 2 the $\gamma\gamma$ partial width of a_2 is determined to be $\Gamma_{\gamma\gamma}(a_2)$=$1.04 \pm 0.06$ KeV. The systematic uncertainties are listed in the following

Inclusive background	7%
M.C. acceptance	10%
Selection cuts	4%
Total	12.5%

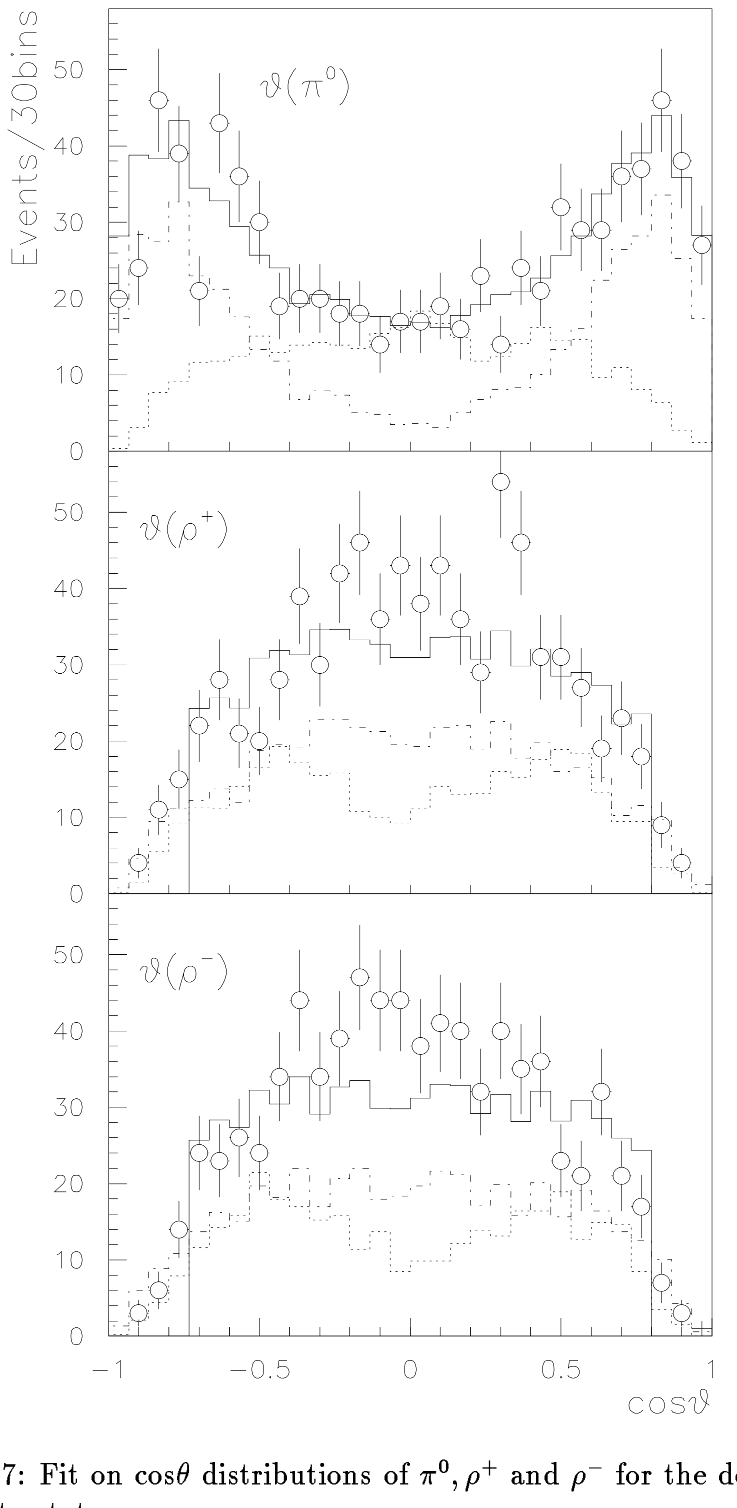

Figure 17: Fit on cosθ distributions of π^0, ρ^+ and ρ^- for the determination of a_2 helicity state.

The uncertainties on the detector acceptance come from the TEC trigger simulation, the TEC track reconstruction efficiency, and the BGO photon detection efficiency. The background comes mainly from inclusive two-photon channels, and the uncertainty on selection includes cuts on E_{BGO}, $(\sum \vec{p}_T)^2$ and ρ band. The radiative width obtained for the a_2 meson is then

$$\Gamma_{\gamma\gamma} = 1.04 \pm 0.06(\mathrm{stat}) \pm 0.13(\mathrm{sys}) \ \ \mathrm{KeV} \tag{6}$$

6 Summary

We have studied the a_2 formation in two-photon interaction by detecting the $\pi^+\pi^-\pi^0$ final state. A least square fit on the center of mass polar angle distribution of π^0, ρ^+ and ρ^- suggests that the fraction of a_2 with helicity $|\lambda| = 2$ is $92. \pm 7.\%$. The a_2 radiative decay width is measured to be $\Gamma_{\gamma\gamma} = 1.04 \pm 0.06 \pm 0.13$ KeV.

References

[1] JADE Coll. J.E. Olsson: Proc. V Int. Conf. on Two-Photon Physics, Aachen 1983 ed. Ch. Berger (Springer, Berlin 1983)

[2] CELLO Coll. H.J. Behrend et al.: Phys. Lett. 114B 378 (1982); Phys. Lett. 125 518 (1983)

[3] PLUTO Coll. Ch. Berger et al.: Phys. Lett. 149B 427 (1984)

[4] TASSO Coll. M. Althoff et al.: Z. Phys. C31 537 (1986)

[5] MARK2 Coll. F. Butler et al.: Phys. Rev. D 42 1368 (1990)

[6] CELLO Coll. H.J. Behrend et al.: Z. Phys. C46 583 (1990)

[7] MD1 Coll. S.E. Baru et al.: Z. Phys. C48 581 (1990)

[8] L3 Coll. B. Adeva et al.: Nucl. Inst. Meth. A289 35 (1990)

[9] F.L. Linde: Charm Production in Two-Photon Collisions, thesis (1988)

[10] A. Buijs et al.: TWOGEN, a Simple Monte Carlo Generator for Two-Photon Reactions, CERN-PPE/93-199 (1993)

[11] V.M. Budnev et al.: Phys. Rep. 15 181 (1975)

[12] W.R.Frazer, J.R. Fulco and F.R. Halpern: Phys. Rev. 136 B1207 (1964)

[13] Particle Data Group: Phys. Rev. D 50 1173 (1994)

[14] J.D. Jackson: Nuovo Cimento 34 1644 (1964)

[15] M.J. Corden et al: Nucl. Phys. B138 235 (1978)

[16] H. Pilkuhn: Relativistic particle physics (Springer, Berlin, 1979)

[17] F. Selleri: Phys. Lett. 3 76 (1962)

[18] see e.g. P. Grassberger and R. Kogerler: Nucl. Phys. B106 451 (1976)